Model Considerations, Calibration Issues, and Metrology Methods for Resist-Bias Models

Edward W. Conrad,[a] Daniel C. Cole,[b] David P. Paul,[a] and Eytan Barouch[b]
[a]IBM Microelectronics, Essex Junction, Vermont, 05452
[b]Dept. of Manufacturing Engineering, 15 St. Mary's Street
Boston University, Boston, Massachusetts, 02215

ABSTRACT

This paper explores the application of phenomenological models that take into account photoresist processing effects when simulating the predicted shapes of small structures created in state-of-the-art microelectronic fabrication. This work extends some of the one-dimensional (1-D) model development reported in recent years to two-dimensional (2-D) structures. A brief overview of the assumptions and background of the relatively simple energy threshold model is given, followed by a more extensive discussion on proceeding beyond this point with more advanced resist "bias" models. A number of subtle, but critical metrology and calibration issues are also discussed including (1) use of SEM top-down micrographs for extraction of measured shape information, (2) calibration of the pixel size associated with the SEM data, (3) use of the measured mask shapes for input to the simulator, (4) evaluation of the projection system focus offset and inclusion of it in the calibration of the model, and (5) the optimization of parameters in the resist-bias model. Typically we have found that after proper calibration of the resist bias model, agreement between predicted and measured shapes for full 2-D structures of 3-σ variation equal to 15 nm can be realized for 248-nm photolithography, for nominal 0.25 μm critical dimensions. Increasing to 0.5 μm defocus typically increases this 3-σ variation to about 40 nm. Further improvements can certainly be expected. Clearly, such predictability can greatly aid in improving the process window for chip design. Some discussion is given on the anticipated pitfalls when extending this approach beyond its region of applicability.

Keywords: Lithography, simulation, development, linewidth, metrology, calibration, phenomenological model, lumped parameter model

1. INTRODUCTION

Several articles have been written in recent years describing the use of fairly simple "resist-bias" models.[1–6] These models extend microlithography aerial image simulation capability beyond the simple "threshold energy model"[7,1,8] that is often used for obtaining a rough prediction for how an optical mask prints. Detailed one-dimensional (1-D) and some two-dimensional (2-D) measurement versus simulation results have been demonstrated with excellent agreement over a range of line widths.[4–6] The 1-D photoresist linewidths predicted with these models correspond to the widths of the bottom edge of long lines and spaces in photoresist, while the 2-D photoresist shapes describe the contour of the bottom edge associated with more general photoresist structures. Here, this work is extended further by presenting full 2-D calibration results for one resist type (UV2HS) over a wide range of photoresist shapes.

The purpose of this paper is several-fold. Previous 1-D modeling work will be extended to 2-D photoresist shapes. In the process of doing this, some of the subtle, but necessary and important calibration and metrology details will be addressed that enable this extension to 2-D shapes. We will also use this work as an opportunity to step back and examine the shift that has occurred in lithography modeling with the introduction of these phenomenological models. In particular, we will examine how and why this approach has worked, what the inherent limitations are, and directions for continued work along these lines will be suggested.

We will discuss the technological needs for modeling and simulation work at different levels of physical sophistication. The models employed here are less detailed and accurate in their physical description than the models that have been conventionally used by microlithography simulation programs such as SAMPLE,[9,10] PROLITH,[11] MCP2&3D,[12,13] and DEPICT,[14] to name a few.

As discussed here, provided that the goals of these different levels of models are kept in perspective, the detailed models and the phenomenological models both provide value, although serving different purposes. The two

approaches are quite different, but each is appropriate to its specific goal and has its own limitations, calibration requirements, and area of applicability.

Section 2 of this paper discusses the direction of lithography modeling. Section 3 begins with a general discussion on phenomenological models, followed by a discussion of the fast phenomenological lithography models recently reported in the literature,[1−6] and the models used in the present work. Section 4 will then provide many of the key points of the paper, including the degree to which the models have been found to fit our measurement data, the predictability of the models, and some of the metrology and calibration concerns that must be addressed if the application of this work is to provide maximum benefit for semiconductor development. At our present level of sophistication in applying these methods, we have typically found that after proper calibration, the shapes of photoresist images can be predicted to within a 3-σ variation equal to 15 nm, for all points on the 2-D shapes. This value applies to 2-D photoresist shapes exposed with 248-nm photolithography for 0.25 μm critical dimension images at zero defocus. Evaluation of samples exposed at 0.5 μm defocus typically increases this 3-σ variation to about 40 nm for our optical exposure conditions of 0.5 for the numerical aperture (NA) and 0.6 for the circular partial coherence parameter. Section 5 illustrates a few points about the line-end-shortening associated with the simple resist bias model used here. Section 6 concludes the paper with some suggestions and a vision for future modeling and calibration work. Given a stable manufacturing process, and adequate systems for calibrating resists and etch processes, the predictability of printing characteristics provided by these modeling procedures should be extremely helpful for improving manufacturing process windows in semiconductor technology. The models should also be useful for incorporating process limitations within more conventional chip design methodologies, thereby bridging some of the gaps that exist between semiconductor process manufacturing and microchip design practices.[15]

2. LITHOGRAPHY MODELING

The approach described in this paper, and in other recent work,[1−6] has a much different aim than conventional microlithography simulation programs.[9−14] Here, we emphasize the reasons for the difference to better place in perspective the benefits and limitations of these methods.

The original work on simulating the formation of photoresist structures[16−18] individually simulated the physical steps involved in the imaging of light in optical projection systems, the exposure of a certain class of photoresist materials, the post-exposure bake step, and the dissolution of the exposed photoresist material. This work was unique because it sought to quantify and model each of the key physical steps involved in forming the patterns in photoresist materials used in microlithography. This simulation work was an interesting mixture of fairly detailed physical mechanisms, such as the imaging of light, combined with much more phenomenological models, such as those pertaining to the chemical reactions during photoresist exposure. The purpose was to make use of the appropriate level of physical description necessary to describe the phenomena with reasonable accuracy. This approach is consistent with the methods that have been used widely in process and device semiconductor simulation work, typically referred to as technology computer aided design (TCAD).[19]

Since this initial work, which greatly helped to quantify the underlying key physical mechanisms involved with photoresist processing, a substantial amount of improvement has been realized in the basic physical models and physical description, the numerical and algorithmic methods, and the interface, output, and ease of use of these programs.[20] Indeed, advanced microlithography simulation programs are now generally believed to (*i*) accurately simulate the physical effects of high numerical aperture optical projection systems, (*ii)* correctly describe the propagation of light into the photoresist structure, while simultaneously solving the change in chemical and optical properties of the resist during the exposure, and (*iii*) properly handle full 3-D photoresist structures, even over steps in the underlying substrates. All of these aspects, and many more, have greatly extended the capabilities of microlithography simulation over the past two decades.

As the dimensions of the structures and the materials comprising them continue to change, new physical considerations that are not currently of first order importance will have to be addressed. It's difficult to predict what the leading order effects may be, but they may include dependence of the effective diffusion coefficients on concentration, consideration of the diffusion of reactants and products during the dissolution process, or the effects of stress within the resist during dissolution. Our present lithography models and physical description are not fundamental enough to make predictions about these behaviors.

The point of this discussion is that although many lithographers think of these models as being "first-principle," they really are not; rather, they include first-principles models along with phenomenological models. These are

combined to give reasonably accurate descriptions of the behavior of the key steps in microlithography. It is quite remarkable that the models work as well as they do, considering the enormous range of time scales involved in the fundamental physical description, including the period of the illuminating light ($\sim 10^{-15}$ sec), the transition rate for chemical bond breaking regarding the photoactive materials ($\sim 10^{-6}$ sec), and the typical exposure time for a photoresist film ($\sim 1 \rightarrow 30$ sec). Of course, one of the reasons why these models work so well is that they involve the accumulation of an enormous number of events, just as the gas law in thermodynamics of $PV = nRT$ is quite accurate, with its underpinnings being due to an enormous number of atomic and molecular collisions. As photoresist structures become sufficiently small that the sizes and numbers of the molecules involved become critical, many of the models used today will need to be revisited.[21]

In our approach, we purposely step back from these advances and attempt to work at a different physical level. As discussed elsewhere,[22] high levels of physical description, such as at the atomic or molecular level, are essential for describing certain phenomena, but become unnecessary, or even undesirable, when dealing with more macroscopic phenomena. In simulation, it is important to clearly recognize when these extra physical attributes are essential, when they are not, and what will be lost by forfeiting this extra detailed physical description. Part of the present discussion is motivated by a panel discussion at SPIE in 1998 that was devoted to the pros and cons of the use of simulation.[23] At this session, technologists discussed the attributes and disadvantages of using full photoresist profile simulators,[9−14] versus the far less intensive programs that use simpler phenomenological models, like those discussed here. We believe this "debate" can readily be resolved by recognizing that the two sets of programs are intended to be quite different.

A photoresist profile simulator simulates the full sidewall profile associated with the development of photoresist. Such a program can be extremely beneficial to a lithographer investigating various process options such as including a top or bottom arc, adjusting the dye content in the resist, adjustment of baking times and temperatures, determining the optimal resist thickness, etc. These programs also provide the means to maximize the process windows associated with these process parameters. The programs will show how the angle of the resist sidewall changes under specific conditions, and how variations in openings developed into the resist are influenced.

The present phenomenological models do not address these points. These models do not contain the detailed physics necessary to make predictions like those suggested above.

Even with these limitations, the phenomenological models are still extremely useful in their own right. They are appropriate for use with fixed lithographic processes where the photoresist chemical makeup, its concentration, thickness, and all the other physical controls involved in the steps of exposure, baking, and dissolution are held reasonably constant. For lithographers interested in comparing the printability of a mask with two photoresist types, or one photoresist type at two thicknesses, these phenomenological models are not helpful, unless separately calibrated for each of these two photoresist processes. In contrast, the detailed photoresist simulators mentioned earlier do yield such predictions.

However, the detailed physical lithography simulators pay a price for such capability; the data volume and the CPU time are enormous for any region of a chip that is large enough to aid a microchip designer. As a rough estimate, consider a 10 μm $\times$ 10 μm region on a chip to be simulated by a detailed photoresist simulator using light with a wavelength of 0.25 μm and a resist thickness of 1.0 μm. Assuming evaluation at five data points in each length of resist equal to the light's wavelength, the number of points required would be $10 \cdot 10 \cdot 1 \cdot \left(\frac{5}{0.25}\right)^3 = 800,000$. Since each location requires several real number values to represent the physical quantities at that point, many megabytes of data volume will result. Scaling this to the size of a chip of 1 cm^2 in area, would result in the utterly impractical data volume of 800 G of points, again, each requiring perhaps 8 bytes of information or more.

In principle, such a calculation on the 10 μm $\times$ 10 μm region is possible using advanced numerical methods for dealing with the required underlying complicated numerical grid, particularly during the dissolution process, and for handling the large data volume involved. However, the computation would daunt even the most powerful of present day computers, and calculation for a full chip is currently utterly impractical. Moreover, the final calculation would produce far more information than a chip designer could reasonably utilize. In addition to information about the bottom of the photoresist structure, it also would contain other information involving the sidewall shapes of each section of a 3-D developed photoresist material.

The intent of the photoresist bias models is to sidestep these difficulties by relying on calibrated phenomenological models that hold over a range of restricted processing conditions. The larger this range, the more useful the models.

We anticipate that new developments and extensions to these phenomenological models will continue for some time as research groups push yet further to improve the accuracy of these models over a larger range of conditions.

3. PHENOMENOLOGICAL MODELS

3.1. General Points

One obvious difference between detailed physical models and phenomenological models is that, speaking only from the physics standpoint, the more fundamental the physical model, the more phenomena the model is capable of accurately describing or predicting. In this sense, for example, the kinetic theory of gases is more fundamental than either the gas law with virial coefficients that relates pressure, temperature, and density, or, as another example, the phenomenological law relating a canon ball's speed through the air to the air resistance on the cannon ball. Neither the gas law nor the air resistance relationship are as physically fundamental as the kinetic theory of gases, because they make no predictions about many properties of a gas, such as the velocity distribution of the gas particles. However, the kinetic theory of gases can be used, in principle, to obtain the gas law and the air resistance relationship. The more fundamental physical relationships enable the phenomenological relationships to be deduced, but not vice versa.

On the other hand, a phenomenological model can be extremely helpful for its intended purpose, that is expressing specific relationships in a very compact and accessible form. To illustrate, both the gas law and the air resistance relationship contain parameters that can be viewed as calibration parameters, such as the virial coefficients and the viscosity. Once the calibration values are known, these relationships provide a significant amount of information. Starting from the kinetic theory of gases to relate pressure to temperature for each new data point would be foolish (*i.e.*, particularly for realistic, nonideal gases), even if powerful computational resources were available.

A second point that in some ways may be obvious, but is often not recognized, is that it is perfectly possible to have two different phenomenological laws that relate the same variables. The first relationship may be more accurate when compared with experiment for one set of conditions, yet less accurate than the second relationship for another set of conditions. In general, we view a phenomenological relationship as being more significant when it is more than just a curve fit, *i.e.* when it also combines some underlying physical knowledge that reduces the number of fitting parameters required to describe the phenomena.

As a simple example, one can deduce by symmetry principles that if a phenomenological "curve fitting" relationship of the form, $F = \sum_{n=0}^{N} a_n s^n$, is used for the resistive force of a projectile moving through the air with a speed s, then $a_n = 0$, exactly, for $n = 0,\ 2,\ 4\ \ldots$, since if s was reversed in signature, then the force F must reverse also. In this case this deduction is obvious; for more complicated situations, such conditions are usually more difficult to recognize.

3.2. General Discussion on Properties

The specific phenomenological model discussed here, and those that have been published elsewhere,[1−6] are only concerned with the prediction of the bottom edge of the developed photoresist structures; these models ignore all other aspects of the topography of the developed photoresist. Why these models work is not immediately obvious. Here we will examine some of these features in general terms and try to explain why these models achieve reasonable results, as well as to examine their potential limitations.

First, one key aspect of these models is that they are based primarily on the aerial image information. For the photoresist structures, this approach seems reasonable, since the aerial image contains considerable information regarding the electromagnetic energy distribution being used to expose the photoresist. However, the aerial image certainly does not contain all the information in this regard, because it isn't sufficient to fully predict the propagational and exposure properties of the fields within the photoresist, particularly for high NA projection systems and thicker films.[24,25] Instead, the aerial image contains only the light intensity information at one plane in the image space of the projection system.

Thus, one immediate consideration is that these models may be tunable to yield good predictions for a given defocus condition, but that without including more detailed information from the incident light field, they should yield lower quality predictions for other defocus values, particularly for thicker resists. Undoubtedly more information

from the incident field, would help to improve this situation. Calibrating these models to include the defocus should therefore be helpful.

A second point is that the aerial image for any single defocus plane, despite not containing all the physical information about fields in the image space of the projection system, still does contain an enormous amount of information. If simulation predictions based on such information match closely with experiment at one optical setting, then they should be expected to also track fairly well as optical parameters are changed (*i.e.*, parameters such as the NA, the partial coherence, or, more generally, the illumination aperture configuration). Unless one changes the optical conditions so much as to enter into a regime where a much different basic physical description is required, changes in the original model settings should be capable of tracking such changes reasonably well. An example of a regime where a different physical description is required, occurs when one proceeds from a low or mid NA situation to a high NA situation; in the high NA case, vector aerial image calculations are required and the propagation of the light into the resist becomes much less of a vertical propagation.

A third observation is that the resist bias and etch bias models that have been developed and reported on so far in the literature[1−6] are generally intended to act as a perturbation to the familiar "threshold model."[7,1,8] The threshold model essentially makes the approximation that any point at the top surface of the resist that receives, during exposure, an incident amount of energy above some threshold value will either develop away, or remain, depending on whether the photoresist is positive or negative. The second main assumption in this model is that the energy received below any surface point on the resist, is proportional to the aerial image intensity.

A number of parameters that are only indirectly related to the detailed physics are being explored by others[1−6] to determine how well they can be utilized to gain some of the predictability that exists in more fundamental simulation approaches.[9−14] A large number of choices exist, including: (*i*) information in the optical image space, sampled from in and out of focus,[3,26] (*ii*) information in the focus plane, but along the direction of the normal to the contour predicted from the threshold model,[1,2] (*iii*) as a "diffused " aerial image[1,5,6] to attempt to account for baking and other "diffusion related" effects, (*iv*) information such as the slope of the aerial image and the maximum peak intensity along a normal to the threshold,[4] or, even (*v*) information like the curvature of the shape predicted by the threshold model. The extent to how well these models work, and for which resist conditions, will undoubtedly continue to be investigated as tests are made, and as new resist processing is developed. Clearly none of these approaches can hope to reproduce the more detailed physical models conventionally used,[9−14] but that is not really the aim; rather, the intent is to find methods that work reasonably well for well controlled processes, and to use these models, with reasonably rapid calibration methods, to find the necessary fitting parameters for the resist process in question.

Next, in contrast with some published articles, etch models should not depend on the aerial image, or, at least only to a slight degree. One might argue that there will be some dependence since the topography of the overlying resist may influence, to some extent, the etching of underlying semiconductor layers, and the topography of the resist is somewhat connected to the aerial image. The size of an opening in resist may play a major role in determining the etch bias of the underlying semiconductor material; since the resist opening is related to the aerial image, then it follows that the etch bias should be indirectly connected to the aerial image. Hopefully, future phenomenological models will be able to make much better advances than this sort of connection, by tying the key etching process parameters to the model's prediction. For our work on etched structures, we use a very simple etch model extension, namely, where the etching process results in a fixed offset to the lithography prediction model, at all points on the contours. Later extensions and experimental investigations could be envisioned where this offset varied, to second order, as a function of curvature and opening predicted by the lithography models, as well as certain etching parameters.

Finally, we note that the key information being used in the present set of models is the aerial image, partly because this is important, and partly because over the past few years several groups have made significant advances in rapid calculation of the aerial image.[27−29,3,8] Certainly, this speed allows a number of new possibilities, including the incorporation of fast calculations into models such as those discussed here, which can be helpful to microchip designers, process technologists, and manufacturing engineers, regarding the exchange of information on processing limitations relevant to the design construction.[15]

3.3. Energy Threshold Model

As mentioned previously, the energy threshold model was a main impetus and often a key starting point for more advanced phenomenological models discussed in the literature.[1−6] It's really a very simple model, yet it includes much of the optical information related to diffraction effects involved with imaging a mask. Moreover, there is a key feature associated with this model that is not always used in the same way. Specifically, we refer to the choice of the contour value of the aerial image that is used to fit measured data; this is the only free parameter in this model. It is common to restrict this parameter to be equal to the energy dose-to-clear in large areas. The choice limits this model, and causes its "predictions" to differ from those of the detailed process simulators more than if this parameter is optimized for the specific photoresist process of interest, and for the family of shapes that are being treated.[30]

For the 2-D case, this single parameter can be used to force the threshold aerial image prediction to agree with the measured shapes at one point in the set of shapes examined. In the 1-D case, one of several different predicted line widths can be forced to the proper value. Used in this way, the aerial image threshold parameter combines all separate controls that actually exist in the photolithography process (such as the exposure, baking, and dissolution times) into a single parameter. By forcing the predicted pattern, such as some critical dimension in Fig. 1, to agree with experiment, the model becomes "tuned" to yield agreement at this point. All other dimensions in the pattern are then determined by the aerial image contour. In a sense, this flexibility with the threshold model actually reflects common experimental procedures, namely, where a set of exposures are carried out for a fixed set of other processing conditions (*e.g.*, baking and dissolution times), and the exposure is then chosen that results in specific structures in the pattern printing with the desired dimension. For the case of a FET gate level, the width of the photoresist structures that pertain to the gate widths are the quantities usually chosen to print at a very specific dimension. All other dimensions in the pattern then fall out as they may, hopefully engineered to be close to their desired design dimension, but they are not *forced* in the exposure process to be a specified dimension; instead, the gate width is the quantity forced to print accordingly.

Thus, there is some flexibility in using the threshold model, namely, the ability to force a key structure to print precisely the desired dimension. One advantage of this approach is that if the set of patterns in the mask all have dimensions close to the critical dimension that was forced to print, then the predictions for all patterns will likely come fairly close to experiment. However, if there is a broad mixture of shapes and dimensions in the pattern, then although the chosen "critical dimension" at some specific point in the pattern will be forced to match experiment well, other points could be significantly off. For example, if the width of a rectangular pattern was forced to agree with experiment, the threshold model could yield poor agreement with the predicted length, particularly if the length to width ratio was much larger than unity. (Of course, once the ratio becomes significantly larger than unity, then the offset between experiment and this threshold model will approach a constant offset, relatively independent of the rectangular length. This constant offset can be significant, however.)

To emphasize this point further, designers and technologists making potential use of this simple model, or in extensions of it, particularly in a CAD tool, should not just blindly use a "30%" or "25%" threshold, but rather force the critical dimensions to print appropriately. The rest of the prediction for the remaining pattern will then fail or succeed according to the model's physical description capability and the degree of calibration of its remaining parameters to the physical process.

3.4. More Advanced Models

References 1-6 describe various approaches to advancing beyond the simple energy threshold model, while still retaining the capability of fast and efficient computational ability. Some very interesting and novel approaches are discussed here. A close similarity is now forming between more detailed lithography simulation models and programs[9−14] and these intentionally designed phenomenological models,[1−6] like that which has existed for some time between detailed process and device simulation programs in microelectronics, *i.e.*, TCAD programs, and the intentionally designed phenomenological and parameterized "compact models" used in microelectronic circuit simulation. TCAD programs are considerably more computationally intensive than these compact models in circuit simulation, yet, as with the more physically based lithography programs, they can predict a much wider range of phenomena.

Today, many groups are working on their own proprietary phenomenological models for their own specific resist and etch processes. Here, we report on a specific set of models found to work with good success for the resist processes and dimensions tested. Improvements beyond these can undoubtedly be obtained, but these models clearly show very useful results just as they are.

Specifically, we have used a "diffused aerial image," so as to attempt to model, to some extent, the effects of the diffusion process during post-exposure baking, as well as "... to account for resolution loss due to other sources."[31] We used a fast aerial image simulator, FAIM,[27,28] and a fast means for calculating the diffusion process, namely, where the convolution with a Gaussian was done by taking the inverse Fourier transform of the product of two Fourier transforms. Specifically, the "diffused aerial image" $I_{\mathrm{D}}(\mathbf{x})$ was related to the aerial image intensity $I_{\mathrm{A}}(\mathbf{x})$ by

$$I_{\mathrm{D}}(\mathbf{x}) = \frac{1}{2\pi L^2} \int_{-\infty}^{\infty} \int_{-\infty}^{\infty} d^2x' \exp\left(\frac{-(\mathbf{x}' - \mathbf{x})^2}{2L^2} \right) I_{\mathrm{A}}(\mathbf{x}') \quad , \tag{1}$$

where L is the "diffusion length parameter" reported in the next section. To clarify, writing this in the form of a 2-D diffusion equation, yields

$$D\left(\frac{\partial^2}{\partial x^2} + \frac{\partial^2}{\partial y^2} \right) I(\mathbf{x}, t) = \frac{\partial}{\partial t} I(\mathbf{x}, t) \quad , \tag{2}$$

which is solved by Eq. (1) when $L = \sqrt{2Dt}$.

A second feature of our modeling approach was to characterize the mask making process[32] and to take the imperfections into account due to mask corner rounding (see, for example, Fig. 1) that typically occur during the mask fabrication process. Here we note that the IBM mask house that we worked with had several mask making processes that could be used, depending on the resolution and turn-around-time required for the application. When the mask fabrication process was very high resolution, and the critical dimensions of the mask were not so aggressive, then of course the need for accounting for the mask corner rounding became essentially negligible. Otherwise, the corrected characterized mask was used as input to the aerial image simulator. This process was fully automated.

Third, there was one other "free parameter," besides the (1) threshold (*i.e.,* contour chosen in the final "diffused image") and (2) "diffusion length" that was calibrated in this modeling work, namely, (3) the defocus value. It is well known that the absolute defocus value in microlithography is a difficult value to ascertain, particularly within a few tenths of a micron; differences from one setting to another are very well controlled, but the absolute value, in relation to the Gaussian image plane, is a much more difficult quantity to know precisely. Moreover, one can certainly legitimately ask, from a modeling standpoint, what is the correct value of defocus to use when calibrating this phenomenological model to fit a set of shapes, particularly when considering photoresist films on the order of a micron in thickness.

We chose to fit our model to the measured photoresist shapes described in the next section at not just one focus setting, but over a range of defocus conditions, where the differences between focus conditions were set by the wafer stage settings, but the single "absolute defocus value" for the family of data was used as a fitting parameter in the model. We found, not surprisingly in hindsight, that this parameter had a similar effect to changes in the diffusion length L in the model, undoubtedly because both parameters act, roughly speaking, to smear the resulting image.

4. CALIBRATION AND METROLOGY ISSUES

A number of subtle, but critical issues arise when moving into the realm of calibrating resist and etch bias models for 2-D shapes, as opposed to the much simpler situation of 1-D structures. The calibration we refer to here is related to the evaluation of model parameters, not to be confused with calibration of SEM measurements. These points we will make generally apply whether considering the models discussed here, or those published elsewhere.[1-6] Properly calibrating 2-D shapes is critical if significant advances in design methods are to be made.[15] All calibration efforts here were made on photoresist and etching processes that were considered stable.

First, we note that it is important to check and characterize the mask-making process and ensure that the masks used have stable processes with regard to important mask characteristics such as mask corner rounding and biases of line edges. Figure 1 shows a scanning electron microscope (SEM) micrograph of a mask made with Etec Systems' ALTA laser beam mask writing tool. This mask was used for the study described here. As can be seen in Fig. 1, although the mask is of high quality, there is a significant rounding of corners that is inherent to this mask making process. The precise SEM measurements of the mask were used in generating our predicted printed shapes, enabling a more detailed calibration of our model to the measured printed images. We note that there have been several mask processes taken into account in the course of our studies. As described elsewhere,[32,33] the mask processes can vary considerably from one semiconductor technology to another, and from one mask level to another within a given

technology. Typically this choice is intentional, since there is a recognized trade-off in the mask accuracy required for a particular semiconductor technology and process level in question, versus the cost and turn-around-time in fabricating the mask.

A word of caution: we found occasionally that when our models did not agree well with SEM measurements of the photoresist structures, or, more precisely, when the agreement was poorer than that to which we had become accustomed, a detailed examination often revealed the mask itself to be the source of the discrepancy. Aside from such mask fabrication "errors," however, we found that average process differences between the mask fabrication process and the design data could be readily accounted for in the modeling process.

Second, the set of shapes chosen for use in characterizing the resist and possible etch processes can be quite important. Generally, sizes and shapes should be selected that best represent the types of patterns used in the lithographic process. This may seem somewhat trivial, but it can certainly be used to strong advantage for fine tuning the models to predict the pattern shapes and sizes for a particular technology.

However, if the lithography process is to be used for very general shapes and patterns, as with random logic, then a broad set of shapes should be chosen for the calibration. The set of shapes shown in Fig. 1 exhibit a wide range of image sizes, shapes, and proximity conditions. In particular, Fig. 1 includes multiple examples of the features of most interest in 2D calibration, namely, line-ends, and corners. A wide range of intensities and intensity-slopes occurs in the aerial image associated with this set of shapes. The ability to model these shapes gives confidence that the models will work well for less demanding patterns. In general, it is important to include shapes that produce aerial image intensities and slopes that encompass the values produced by the critical shapes in the product pattern to be exposed.

Nine of the shapes in Fig. 1 were selected for calibration purposes, namely, all but those in the bottom right of the figure. The calibration shapes included the three "T" shapes shown, as well as six of the seven "bar" shapes. For our choice of photoresist, stepper parameters, and resist processing conditions, the smallest bar in Fig. 1 was poorly resolved and exhibited residual resist. For this reason, it was omitted from this study. However, the calibration shapes included the smallest dimensions used in the lithographic process being characterized. The "T" shapes in Fig. 1 ensured that "inside" and "outside" corners were included in the calibration, as well as horizontal and vertical shapes. The smaller "contact" bars ensured that shapes with low maximum aerial image intensity and small slopes were included. These nine shapes, with 0.25 μm minimum critical dimensions, along with seven similar "T" and "bar" shapes with 0.35 μm critical dimensions, were used to calibrate our 0.25 μm UV2HS lithographic process.[34]

Another point important to our resist-bias calibration procedure is related to the defocus of the projection tool. Data was included for a range of defocus conditions. Figure 2 was taken to be nominally in focus, while Fig. 3 was $+0.5$ μm different in focus with respect to the condition in Fig. 2. The absolute focus value was adjusted by a fixed focus offset that was treated as an adjustable parameter that was used to fit simulation to experiment. We were unable to get consistent agreement between experiment and simulation without adjustment of this parameter. The defocus levels used in the calibration ranged from approximately -0.50 μm to $+0.50$ μm. The range of focus chosen for calibration purposes should depend on the choice of projection tool parameters and the critical dimensions of interest. We chose a fairly large range of focus due to the 0.25 μm critical image size and the 0.5 NA of the Micrascan II used in this study.

Next, we note that the setup of the SEM and edge detection associated with the SEM pictures needs to be carefully taken into account. One needs to choose beam currents, accelerating voltages, and magnifications appropriate to the goals of the study from both a picture quality and image resolution point of view. Also, careful attention to SEM astigmatism and focus is essential to obtain high quality data.

Data presented here was collected with a JEOL 6600 metrology SEM. Photoresist structures at the wafer level were measured using an accelerating voltage of 12 KV, a magnification of 25 KX, and a beam current in the range of 3-5 pA. The working distance was 15 mm; a single ET detector was used. Mask images were measured on this same SEM at an accelerating voltage of 10 KV, a magnification of 6 KX, and a beam current of $1-3$ pA. A micro channel plate detector was used. For both mask and wafer measurements, 150 frames were integrated to reduce noise.

One problem occasionally noticed with SEM data, particularly when working with verifying some of the shapes in related SRAM work,[15] was that it was fairly easy to have a situation where the SEM signal was in saturation on some edges of structures. Signal saturation (or intensities at the maximum recorded value) results in loss of edge definition and is a factor that must be avoided.

Another important point on the metrology/calibration issues of this modeling work has to do with the cost function. The cost function provides a metric of the agreement between the measured and simulated shapes. Here, there are many choices to be considered, such as assignment of weights of data through focus and exposure, and whether to assign different weights for different images in the set of sampled shapes. Regarding the latter, there are many possibilities here, such as weighting most heavily the sections of the patterns that are considered most critical. Thus, one might desire to more heavily weight the gate regions of FET patterns and to weight very little the corner regions on contacts. Moreover, one needs to decide whether long straight regions, such as the longer rectangular pattern in the upper right of Fig. 2, should be weighted equally, less than, or more than the other smaller structures in this set of patterns.

These possibilities were noted and considered carefully. For the purposes of the present study, we chose to weight each shape in the set of patterns equally. For the nine shapes in Fig. 2, this procedure seemed fairly reasonable, since the sizes of the nine shapes were not enormously different from each other, as could occur in yet more general random logic situations.

The calculation of our cost function was achieved by partitioning each of the shapes into a large number of equal length segments, independent of the length of the shape's perimeter, thereby treating each shape equally in importance. Once the fragmentation of the perimeter of the shapes was achieved, the distance between corresponding segments of the measured and simulated shapes was calculated. The sum of the squares of the distances between corresponding segments over all shapes, all focus values, and all exposures, defined the cost function.

The distance between corresponding segments was typically on the order of a few tens of nanometers. We generally recorded shapes over an SEM field of view of 4 to 10 μm, with individual shapes often having extent in one direction of at least 1 μm. Since the errors were typically much less than 1% of the field of view and difficult to distinguish with a simple overlay of the shapes, it was helpful to magnify the error in our data presentation to aid in identifying the detailed character of the differences between simulation and measurements.

Plots such as the one shown in Fig. 4 were used to represent and analyze the distribution of distances and directions between corresponding simulated and measured points. The length of the vectors in Fig. 4 are scaled to the magnitude of the differences between simulation and measurement, thereby allowing for easy identification of the regions of largest deviation. Probing into the source of the regions of large deviations often resulted in the identification of a mask error, a poor SEM signal, or a poor quality resist edge.

The upper left hand corner of Fig. 4 contains a summary of the distribution of vector lengths. For example, the "100>0 nm," "87>5 nm," and "72>10 nm" specifications indicate that 100 vectors were contained in the plot, $(100 - 87) = 13$ of them with lengths less than 5 nm, $(87 - 72) = 15$ of them with lengths between 5 and 10 nm, etc. The "3 Sigma" designation in the lower left indicates the value of 3-σ standard deviations for the data. The maximum vector length can be found in the lower right of the plot, which here was 27 nm.

Figure 5 demonstrates the results when the plot is expanded to include a larger number of shapes. Here, 4500 measurements of the difference between simulation and experiment are displayed. Consequently, individual vectors cannot be distinguished. However, the width of the band along with the darkness of the line provides an indication of the magnitude of the errors.

Another point we want to mention here was found to be particularly important. In our resist calibrations that made use of data from many different SEM micrographs, we found a large variation in systematic SEM errors. Specifically, we found errors in magnification and orthogonality far beyond the few parts-per-million that would be expected from mask errors and projection tool contributions. Although these errors are typically on the order of a percent or so, it is important to realize that over a 10 μm field of view, a 1% error can result in a 100 nm error. Since we are attempting to characterize edge locations to less than 10 nm, SEM calibration is then clearly a critical issue and must be controlled to within about 0.1% over these size regions.

Accounting for SEM errors can be achieved by incorporating targets with known right angles and known pitches in the field of view. Alternatively, the calibration can be achieved with a separate SEM calibration sample imaged under identical conditions to those used for measurement of the resist samples.

Figure 6 shows the agreement between measurement and simulation over the entire field of view using the raw SEM data as normally calibrated. Note that the image of the lower left shape was used to register the two sets of data. In this figure, SEM data was adjusted for translational offsets and rotation only. Some images show a fairly strong systematic mismatch in their positions. Careful examination of the plot indicates that much of the error can

be accounted for by introducing additional small changes in first order systematic terms (*i.e.,* different magnification corrections in the x and y directions, and orthogonality).

Figure 7 shows the agreement after adjustment of these systematics by about 1% or less. Although differences can still be seen, they are greatly reduced from those observed in the absence of the fine tuning of the SEM calibration. The differences shown here are probably largely due to inaccuracies in our model and edge detection, as opposed to pixel calibration errors with the SEM.

Most SEM analyses are concerned with the measurement of small structures over small fields of view. As can be seen here, however, when comparing shapes of many small structures over large fields of view, the importance of accurately calibrating the SEM measurements becomes much more significant.

Another point we wish to mention regarding the analysis of these shapes, is that when images are exposed sufficiently far out of focus, or with improper exposure conditions, they of course print poorly. This may include bridging of images, but more commonly results in residual photoresist at the bottom of spaces, or failure of the image to print at all. If the simulation predicts they still will print, then one must decide what to do about how to weigh the error, since here, according to the earlier definition of the error difference, one has a larger degree of ambiguity on how to assess this error. For the purpose of this study, we chose to review the quality of the images through the range of focus of interest and avoided inclusion of images that printed poorly in the analysis.

Figure 8 shows the overlay of measured and simulated images for the +0.75 μm defocus condition. Note that the number of images is reduced. This result is due to bridging of the two images in the upper right of this figure, at this defocus condition.

Figure 9 is the corresponding vector plot of the difference between simulation and prediction for this +0.75 μm defocus condition. Note that some systematic errors still appear to be present, as there is a general tendency for vertical deviations to be positive (*i.e.,* vertical dimensions tend to be at the predicted size or larger) while horizontal dimensions tend to be negative (*i.e.,* horizontal spaces tend to be at nominal dimension or smaller). This behavior isn't totally surprising since lens aberrations were not taken into account in this study. The observed behavior is consistent with the presence of a small amount of astigmatism in the stepper lens.

We found the agreement of model to prediction to be much better for positive defocus values than for negative defocus. Figure 10 is typical of the image quality for the negative focus condition. Figure 11 shows the associated vector plot of the errors. Our resist bias model used here is not sufficiently sophisticated to treat positive and negative focus differently. Results clearly indicate that additional model considerations must be included to account for the observed asymmetry about focus of image shapes, which is a well known effect.[24,25]

5. DESCRIPTIVE CAPABILITY OF PRESENT MODEL

The previous section addressed a number of subtle, but necessary, points to take into account when comparing simulation predictions of 2-D top-down photoresist shapes with SEM measurements. Although a number of fast, phenomenological resist bias models have been recently described in the literature, and compared with extensive 1-D measurements, this paper concentrated on general methods for calibrating and making comparisons for 2-D structures, as applied to one specific set of models. Here, a "diffused" aerial image model with a threshold was used. Mask shape effects were taken into account in these calculations. For etch effects, we have considered only a constant etch bias from the predicted photoresist shape, where different etch processes may provide biases of different amounts, as well as positive or negative directions from the resist shape.

Here we demonstrate how the present set of simple models typically accounts for some of the key effects normally found with 2-D resist shapes. Figure 12 illustrates the key point. In this figure, three models are compared for one of the "T" shapes in Fig. 1. The rectangular shape is the intended design shape. The next curve inside the design shape is the prediction from an aerial image calculation, assuming a threshold value where the widths are forced to print at the prescribed critical dimension. As can be seen, this first-order model does predict shortening of the lengths, as typically observed; however, as is well known, this threshold model does not account for the full effect observed.

The middle curve in Fig. 12 is the prediction obtained with the aerial image-threshold model when mask shape errors are accounted for. The figure shows that this factor can be significant.

Finally, the inner most curve is the predicted shape for a diffused aerial image, with mask error corrections, and the choice of threshold that forces the simulation to print the proper critical width. As compared with measurement

data, as seen in the earlier figures, this set of models does indeed yield good agreement with the resist data we have tested. These three effects are seen to be significant in terms of providing fairly accurate modeling of the shortening of printed shapes with long length to width ratios.

6. CONCLUDING REMARKS

This paper included a rather broad discussion of the motivation, aim, and direction of developing phenomenological models for predicting the bottom edge of developed photoresist structures in semiconductor microelectronics. These models are in contrast to the more fundamental work that has been in progress for over two decades on the modeling of key physical steps involved in microlithography. With proper calibration, these new models are fairly accurate, and computationally fast, which is their key advantage. However, because these models are phenomenological, calibration of the model parameters is required. The calibration of these models is effective when the lithographic and etching processes are well controlled and quite stable.

A number of subtle, but important, metrology and calibration issues need to be examined in order to best make full use of these models. One specific application of these models is discussed elsewhere,[15] and serves as an example of how these fast calculational models can significantly aid in the communication and inclusion of process effects into the microchip design.

Here we have described the calibration steps we followed, including the general features of a software analysis system, for obtaining the model parameters of a photoresist process. A relatively simple diffused aerial image model was used, with an adjusted threshold. Mask corner rounding effects were also included. An adjustable defocus offset value was allowed when fitting the data over a range of defocus conditions, where the differences in defocus were prescribed by the focus system of the projection tools. For the cases examined, we were able to generally predict to within a 3-σ variation, the edge of 2-D photoresist shapes for 248 nm photolithography, within 15 nm on all points of the resist shapes, for nominal 0.25 μm critical dimensions. Increasing to 0.5 μm out of focus increased this 3-σ value to about 40 nm.

We believe measurement procedures similar to those described here can be extremely useful to semiconductor manufacturers for characterizing resist and etch processes. The analysis tools, once set up, are not difficult to maintain. As new processes are developed, they can be characterized by these methods and used for strong predictive purposes. At the very least aid, these methods can aid with design-rule specification. With more aggressive changes in interactions between design and technology practices, such methods can be applied even more effectively by incorporating them tightly into the design phase.[15]

As with all phenomenological models, care must be taken when extending the model predictions outside their range of predictability, since the models are highly reliant on well-calibrated procedures. Thus, when exploring new photoresist processes and materials, the tools included in more conventional microlithography simulation programs[9−14] are preferable. However, for well-controlled and characterized processes, the present models can be extremely helpful for predicting proximity process effects and addressing many of them in the circuit layout design stage, or in post-processing steps.

ACKNOWLEDGMENTS

E. Barouch and D. Cole acknowledge that work was supported in part by DARPA and AFOSR.

REFERENCES

1. T. A. Brunner and R. A. Ferguson, "Approximate Models for Resist Processing Effects," in *Optical Microlithography IX*, G. E. Fuller, ed., *Proc. SPIE* **2726**, pp. 198-207, 1996.
2. J. Li, "Model-based Optical Proximity Correction Including Effects of Photoresist Processes," in *Optical Microlithography X*, G. E. Fuller, ed., *Proc. SPIE* **3051**, pp. 643-651, 1997.
3. N. Cobb, A. Zakhor, and E. Miloslavsky, "Mathematical and CAD Framework for Proximity Correction," in *Optical Microlithography IX*, G. E. Fuller, ed., *Proc. SPIE* **2726**, pp. 208-222, 1996.
4. N. Cobb and A. Zakhor, "Experimental Results on Optical Proximity Correction with Variable Threshold Resist Model," in *Optical Microlithography X*, G. E. Fuller, ed., *Proc. SPIE* **3051**, pp. 458-468, 1997.

5. J. Zhao, J. Garofalo, J. Blatchford, E. Ehrlacher, and E. Nease, "Applications of Enhanced Optical Proximity Correction Models," in *Optical Microlithography XI*, Luc Van den hove, ed., *Proc. SPIE* **3334**, pp. 234-244, 1998.
6. C.-N. Ahn, H.-B. Kim, and K.-H. Baik, "A Novel Approximate Model for Resist Process," in *Optical Microlithography XI*, Luc Van den hove, ed., *Proc. SPIE* **3334**, pp. 752-763, 1998.
7. A. Rosenbluth, D. Goodman, and B. J. Lin, "A Critical Examination of Submicron Optical Lithography Using Simulated Projection Images," *J. Vac. Sci. Technol. B* **1** (4), pp. 1190-1195, 1983.
8. D. A. Bernard, J. Li, J. C. Rey, K. Rouz, V. Axelrad, "Efficient Computational Techniques for Aerial Imaging Simulation," in *Optical Microlithography IX*, G. E. Fuller, ed., *Proc. SPIE* **2726**, pp. 273-287, 1996.
9. W. G. Oldham, S. N. Nandgaonkar, A. R. Neureuther, and M. M. O'Toole, "A General Simulator for VLSI Lithography and Etching Processes: Part I - Applications to Projection Lithography," *IEEE Trans. Electron Devices* **ED-26** (4), pp. 717-722, 1979.
10. K. K. H. Toh, A. R. Neureuther, and E. W. Scheckler, "Algorithms for Simulation of Three-Dimensional Etching," *IEEE Trans. CAD*, **CAD-13** (5), pp. 616-624, 1994.
11. C. A. Mack, *Inside Prolith : A Comprehensive Guide to Optical Lithography Simulation*, FINLE Technologies, Inc., 1997.
12. E. Barouch, B. Bradie, U. Hollerbach, S. A. Orszag, and M. Peckerar, *IEEE Electron Device Lett.* **EDL-12**, pp. 513-515, 1991.
13. E. Barouch, U. Hollerbach, S. A. Orszag, C. R. Szmanda, J. W. Thackeray, "Simulations of Bar Printing Over a MOSFET Device Using I-line and Deep-UV Resists," in *Optical/Laser Microlithography IV*, V. Pol, ed., *Proc. SPIE* **1463**, pp. 464-474, 1991.
14. S. Brainerd, D. Bernard, J. Rey, J. Li, Y. Granik, and V. Boksha, "Sub-half Micron Contact Window Design with 3D Photolithography Simulator," in *Optical Microlithography X*, G. E. Fuller, ed., *Proc. SPIE* **3051**, pp. 552-566, 1996.
15. D. C. Cole, O. Bula, E. W. Conrad, D. S. Coops, W. C. Leipold, R. W. Mann, and J H. Oppold, "Optimization Criteria for SRAM Design - Lithography Contribution," in *Optical Microlithography XII*, Luc Van den hove, ed., *Proc. SPIE* **3679**, (in print) 1999.
16. F. H. Dill, "Optical Lithography," *IEEE Trans. Electron Devices* **ED-22**, pp. 440-444, 1975.
17. F. H. Dill, W. P. Hornberger, P. S. Hauge, and J. M. Shaw, "Characterization of Positive Resist," *IEEE Trans. Electron Devices* **ED-22**, pp. 445-452, 1975.
18. F. H. Dill, A. R. Neureuther, J. A. Tuttle, and E. J. Walker, "Modeling Projection Printing of Positive Photoresists," *IEEE Trans. Electron Devices* **ED-22**, pp. 456-464, 1975.
19. D. C. Cole, E. M. Buturla, S. S. Furkay, *et al.*, "The Use of Simulation in Semiconductor Technology Development," *Solid-State Elec.* **33**, pp. 591-623, 1990.
20. On the latter point, see, for example, the recent Java interface work reported by C. Hsu, R. Yang, J. Cheng, P. Chien, V. Wen, and A. R. Neureuther, *Optical Microlithography XI*, Luc Van den hove, ed., *Proc. SPIE* **3334**, pp. 197-201, 1998.
21. Perhaps the advances being made into nanoelectronics will warrant some of these concerns.
22. See, for example, Sec. IIB in Ref. 19 for a discussion on the different physical levels of description that have been used for probing the very microscopic to more macroscopic aspects of a phenomena as apparently as "simple" as diffusion.
23. An evening panel session on the use of simulation in photolithography was held at SPIE's 23rd Annual International Symposium on Microlithography, in Santa Clara, CA, on 2/24/98.
24. M. S. Yeung, "Modeling High Numerical Aperture Optical Lithography," in *Optical/Laser Microlithography*, B. J. Lin, ed., *Proc. SPIE* **922**, pp. 149-167, 1993.
25. D. A. Bernard and H. P. Urbach, "Thin-Film Interference Effects in Photolithography for Finite Numerical Apertures," *Journal of the Optical Society of America A*, **8** (1), pp. 123-133, 1991.
26. J. Garofalo, J. DeMarco, J. Bailey, J. Xiao, and S. Vaidya, "Reduction of Asic Gate-Level Line-End Shortening by Mask Compensation," in *Optical/Laser Microlithography VIII*, T. A. Brunner, ed., *Proc. SPIE* **2440**, pp. 171-183, 1995.
27. D. C. Cole, E. Barouch, U. Hollerbach, and S. A. Orszag, "Derivation and Simulation of Scalar Aerial Images for Higher Numerical Apertures," *Jap. J. Appl. Phys.* **31**, pp. 4110-4119, 1992.

28. E. Barouch, D. C. Cole, U. Hollerbach, S. A. Orszag, "Vector Aerial Image with Off-Axis Illumination," in *Optical/Laser Microlithography VI*, J. D. Cuthbert, *Proc. SPIE* **1927**, pp. 686-708, 1993.
29. Y. C. Pati and T. Kailath, "Phase-Shifting Masks for Microlithography: Automated Design and Mask Requirements," *Journal of the Optical Society of America A*, **11** (9), pp. 2438-2452, 1994.
30. See, in particular, Sec. 2 in Ref. 1. Here, the threshold model is compared directly with a full lithography simulation using PROLITH, where the threshold energy is taken as being the dose to clear in large clear regions. Fig. 2 here clearly shows the poor results that a simple application of the threshold model will yield if the threshold energy parameter is literally interpreted in this manner.
31. See p. 203 in Ref. 1.
32. W. Leipold, F. Baker, O. Bula, R. Leidy, and A. McGuire, "Polysilicon Line End Resolution Enhancement: Improving Yield on IBM's Current and Future Technologies," *IBM MicroNews* **4** (3), pp. 19-23, 1998.
33. Also see Fig. 1 in Ref. 15.
34. Studies since this work have used additional sets of shapes with more systematic variations; nevertheless, even a "potpourri" of shapes such as those used in Fig. 1 were found to serve as an excellent calibration tool.

FIGURES

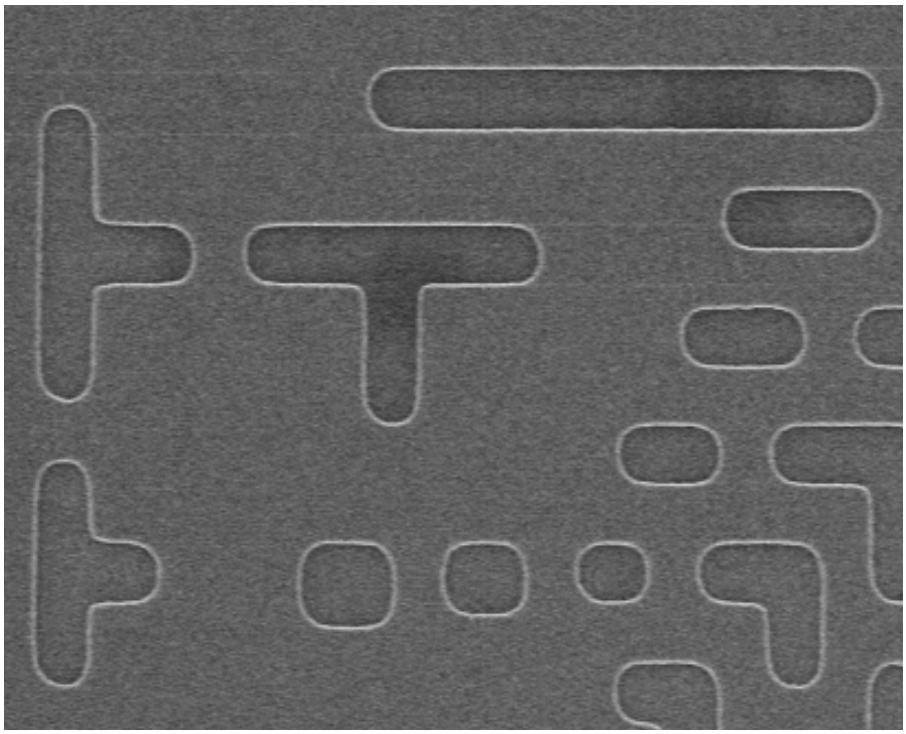

Figure 1. SEM micrograph of an optical projection reticle. The CAD design data for these structures had 0.25 μm as the smallest dimension in "wafer dimensions," or 1.0 μm on the mask (4X projection system). In wafer coordinates, the region shown here was roughly 3.0 μm by 3.5 μm. The long bar on the top right was 2.0 μm long.

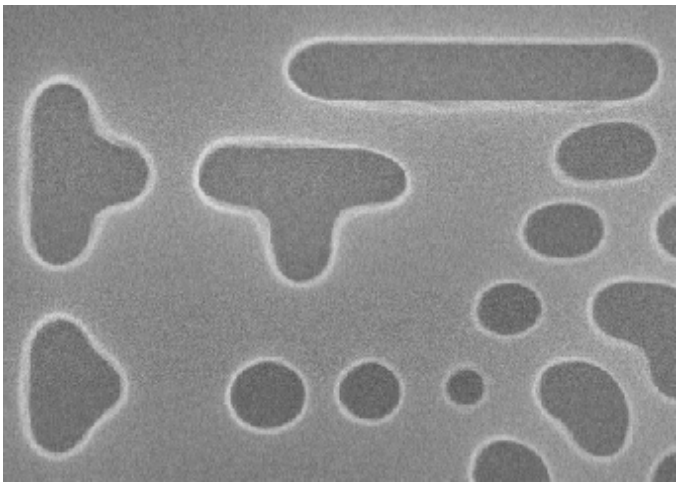

Figure 2. SEM of UV2HS photoresist structures, corresponding to the mask pattern shown in Fig. 1. The nominal focus setting used here was 0.0 μm from the Gaussian image plane.

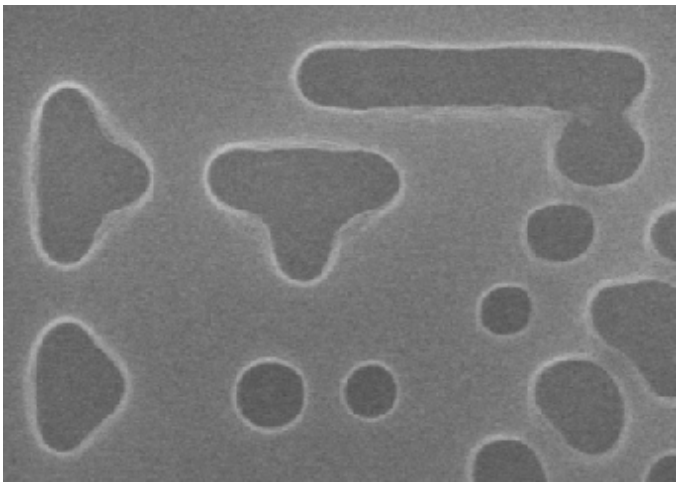

Figure 3. SEM of UV2HS photoresist structures, corresponding to the mask pattern shown in Fig. 1. The nominal focus setting used here was 0.75 μm from the Gaussian image plane. As can be seen, the smallest structure in the bottom right of Fig. 1 does not print at this defocus condition.

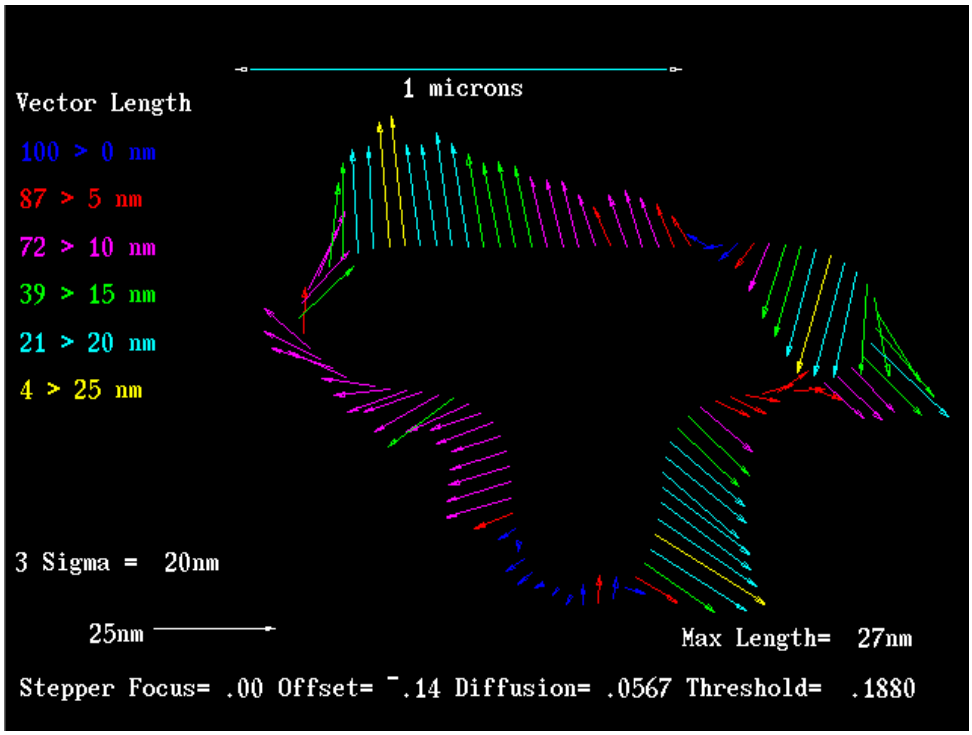

Figure 4. Vector plot of the deviations between simulation and SEM measurements corresponding to one of the UV2HS printed "T" shapes in Fig. 1.

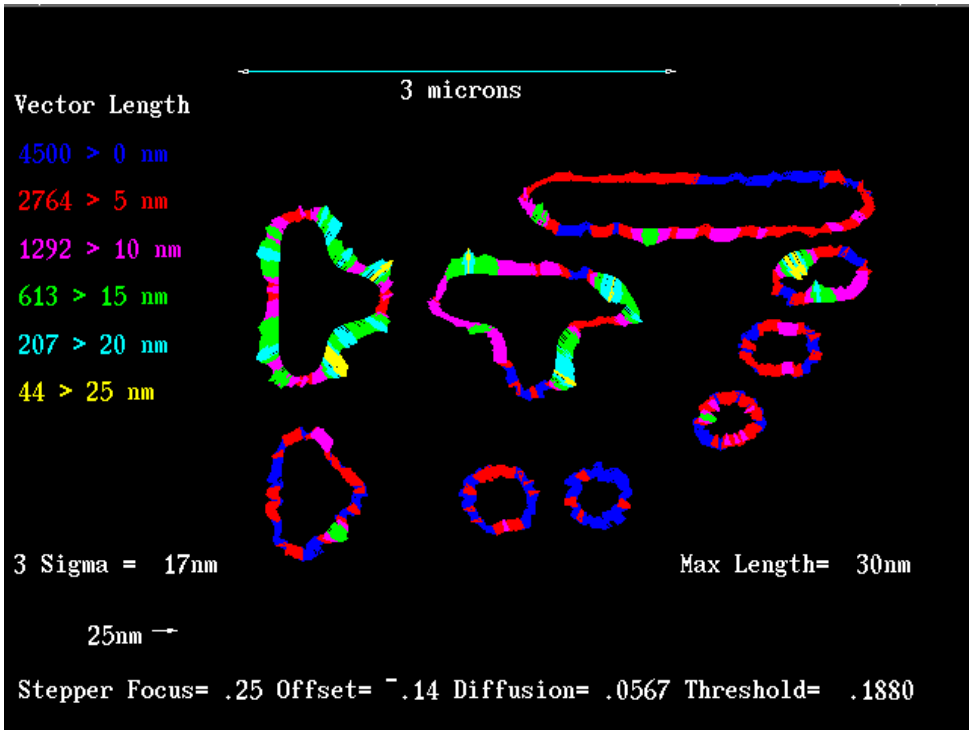

Figure 5. Plot showing the differences between the SEM detected edge of the resist structure in Fig. 2 and the simulated predictions. We normally display this plot in color, with each set of vectors having a separate color, as this scheme helps to more quickly discern the regions of largest differences.

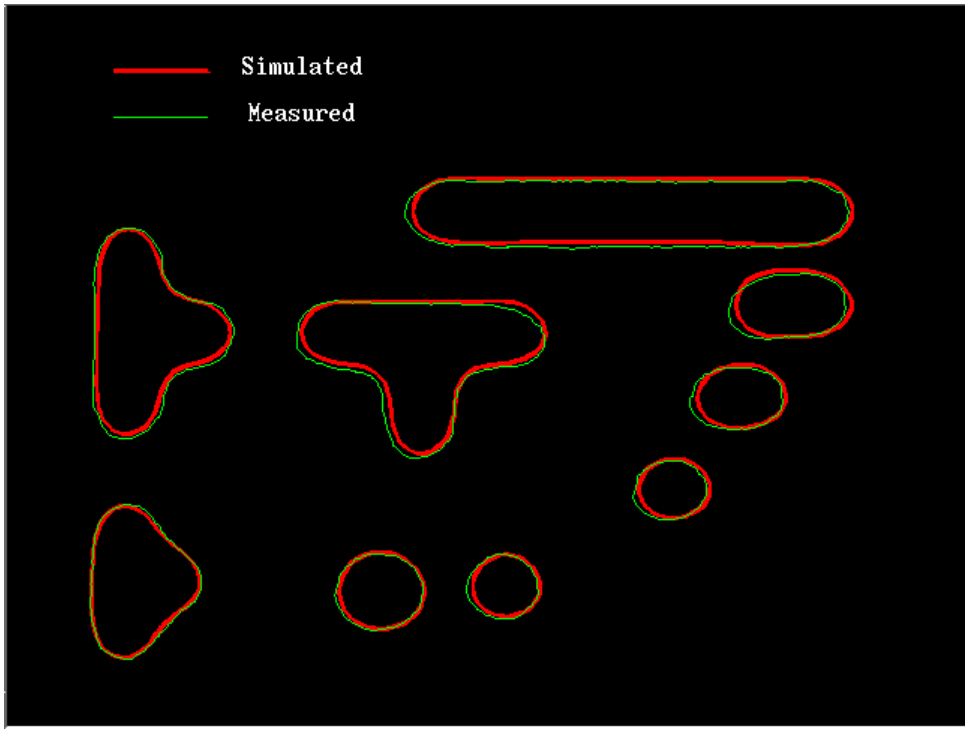

Figure 6. Superposition of simulation and measurement for the in-focus case of nine of the photoresist shapes in Fig. 1. The contours were aligned to agree for the bottom left shape. As can be seen, the remaining shapes become increasingly separated the farther away they are from the bottom left shape. SEM calibration and distortion account for the difference.

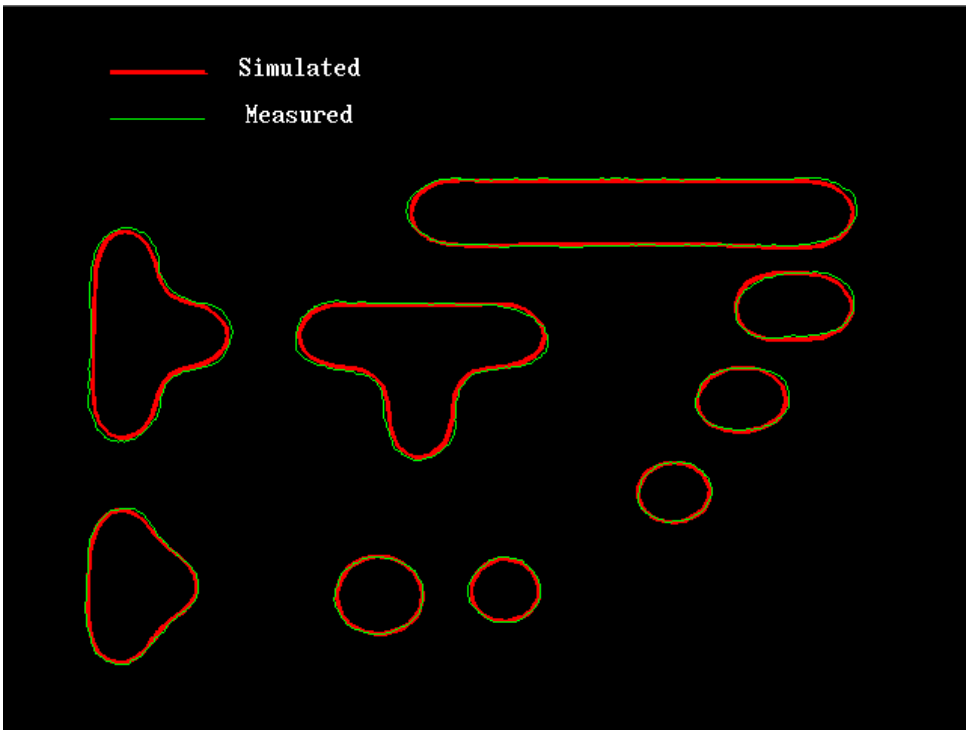

Figure 7. Superposition of simulation and measurement for the in-focus case of nine of the photoresist shapes in Fig. 1, with first-order systematic calibration errors taken into account in the SEM data. As can be seen when compared with Fig. 6, the agreement is considerably improved.

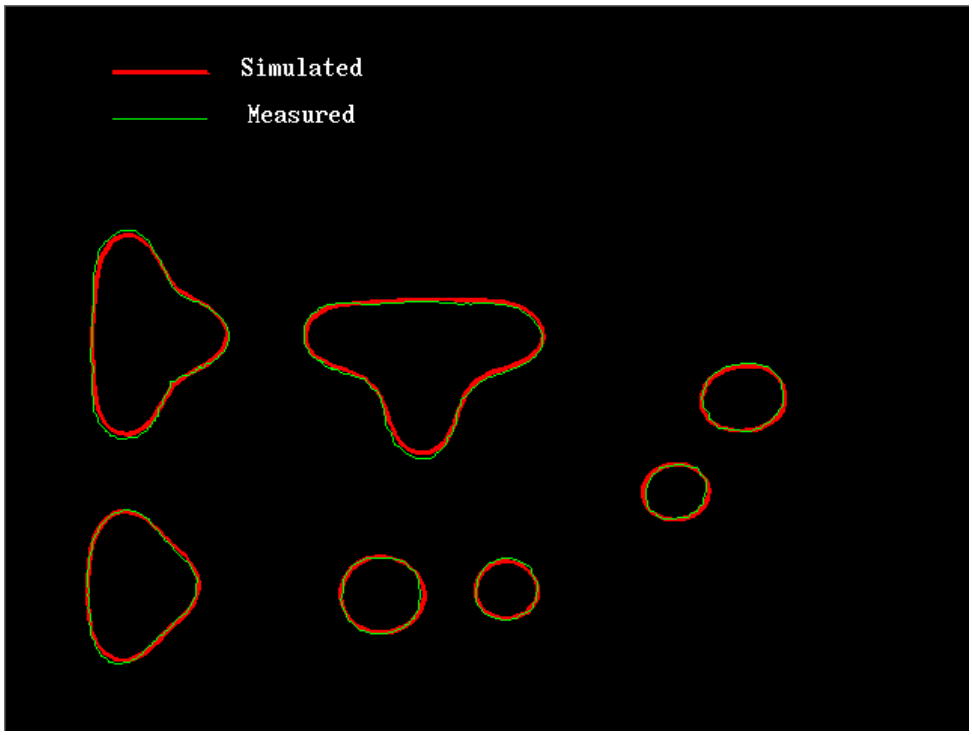

Figure 8. Comparison between SEM measurement of UV2HS structures and simulation at 0.75 μm defocus.

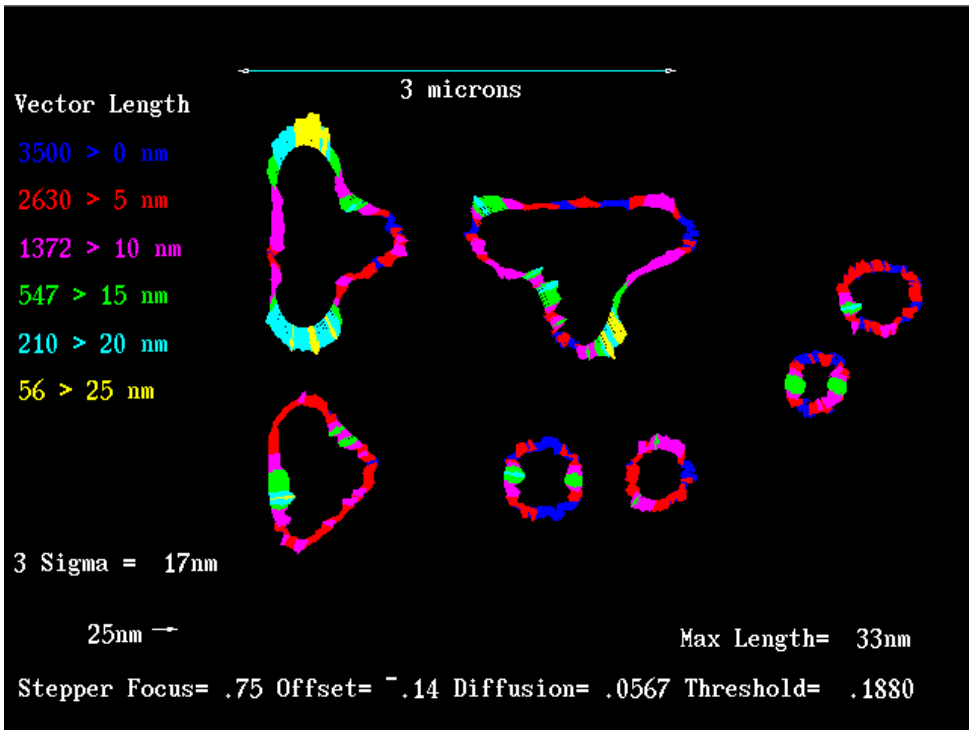

Figure 9. Vector plot of differences between simulation and experiment corresponding to the two contours shown in Fig. 8. Defocus equals +0.75 μm.

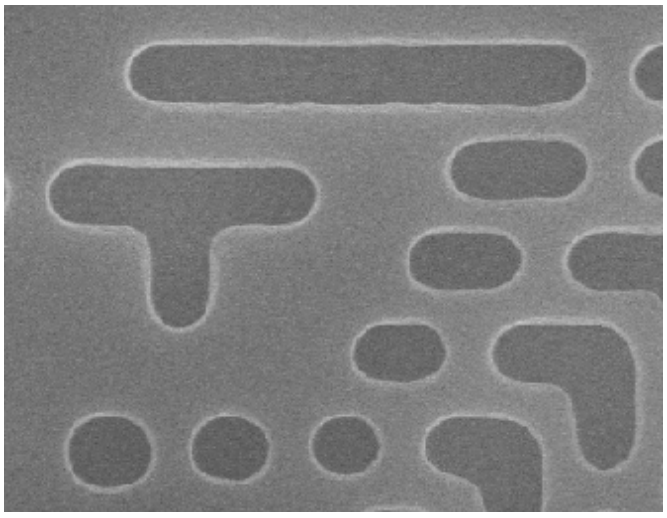

Figure 10. SEM picture of 0.35 μm images for -0.5 μm defocus.

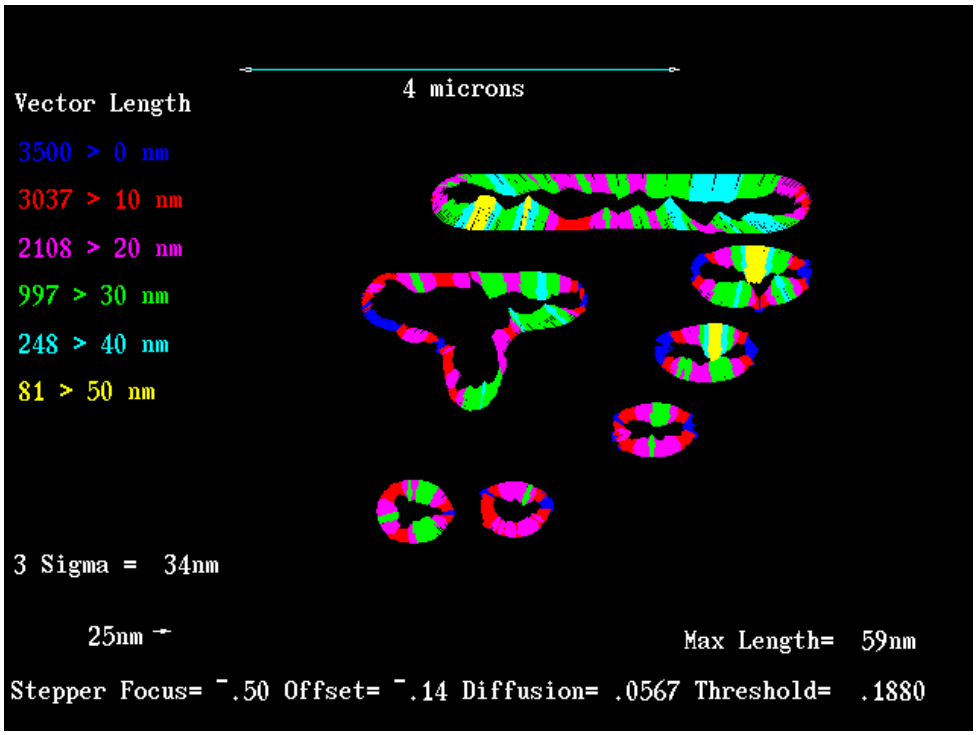

Figure 11. Vector plot of differences between simulation and experiment corresponding to Fig. 10. Defocus equals -0.5 μm.

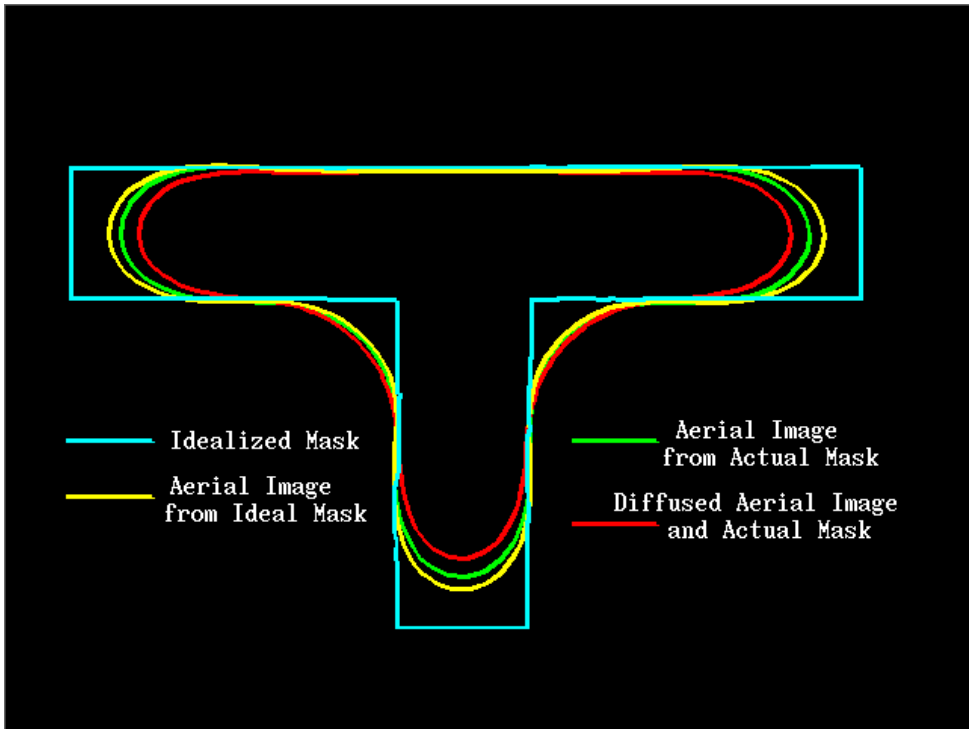

Figure 12. Superposition of predictions from a threshold aerial image model (outside curve), versus the threshold aerial image model with mask corrections (middle curve), versus a diffused aerial image threshold model, with mask corrections (inner curve).